Chapter 2
Mode-Locked Laser Model

2.1 Introduction

Various models exist for passively mode-locked lasers, each with their own advantages and restrictions. One of the earliest models was based on a master equation approach, developed by Haus, which allows the mode-locked pulses to be described analytically under the assumption of only small changes in the gain and losses per cavity round trip [1]. This approach works well for solid state lasers, however the assumption of small changes in the gain and losses per round trip is not applicable to semiconductor lasers. For accurate modelling of semiconductor passively mode-locked lasers, finite-difference travelling-wave models are typically used [2–10]. However the numerical integration of such models is computationally very expensive and this makes it infeasible to use such an approach to study the influence of feedback over a wide range of feedback delay times. In [2, 3, 9], the impact of feedback is studied, but in each case only in the regime of short feedback cavities. An alternative modelling approach is to use a delay differential equation (DDE) model. This was first proposed in [11, 12] and extended to include optical feedback in [13]. This approach assumes a ring cavity geometry with unidirectional propagation and uses a lumped element method to include non-resonant losses and spectral filtering. Using this model the computational cost is greatly reduced and feedback can easily be incorporated. However, the simplifying assumptions mean that this model is strictly only applicable to ring cavities, whereas linear cavity geometries are commonly used for monolithic passively mode-locked semiconductor lasers. Despite this limitation most of the qualitative trends, especially in dependence of feedback parameters, are very similar to experimental results for linear cavities [14–18]. Due to its suitability to studying optical feedback, we will use the DDE model in this thesis.

The modelling of the charge carriers is dependent on the choice of semiconductor material and can be done to varying degrees of complexity [6, 12, 19–22]. We will use a simple model for a quantum-well gain medium. Despite this, in subsequent chapters we will compare our results with experiments using quantum-dot lasers and

L. Jaurigue, *Passively Mode-Locked Semiconductor Lasers*, Springer Theses,
DOI 10.1007/978-3-319-58874-2_2

show that the qualitative dependence on the feedback parameters is captured by the DDE model.

This chapter is structured as follows. In Sect. 2.2 we present the derivation of the DDE model. Then in Sect. 2.3 we discuss the assumptions that underlie this model. We also discuss key differences that arise compared with travelling wave models, as well as extensions that have been made to this model.

2.2 Derivation of the DDE Model

In this section we present the derivation of the DDE model for a passively mode-locked semiconductor laser which is introduced in [12, 23]. In [13] the model is extended to include optical feedback from one external cavity. Here we present extension to multiple feedback cavities. The derivation follows those of [13, 24].

The light-matter interaction needed for lasing to occur can be described using a semi-classical theory [19, 25]. In this approach the light field is described classically, but the motion of the charge carriers is described quantum-mechanically. Although the quantum-mechanical treatment of the carriers is necessary for lasing to be described, the classical treatment of the light field is sufficient when considering devices that involve macroscopic numbers of charge carriers and photons. The results of the semi-classical theory are the Maxwell–Bloch equations, which describe the evolution of the electric field, the charge carrier inversion and the microscopic polarisation. The derivation for a simple two-level system is given in [25]. For a semiconductor gain medium the derivation is somewhat more complicated due to inhomogeneous broadening (distribution of charge carrier kinetic energies), many-body Coulomb interactions and carrier–phonon interactions. A comprehensive derivation of the semiconductor Bloch equations is given in [19].

We will start the derivation of the DDE model directly from the standard travelling wave model for semiconductor quantum-well lasers [26–28]:

$$\pm \frac{\partial \mathcal{E}_r^{\pm}(t,z)}{\partial z} + \frac{1}{v}\frac{\partial \mathcal{E}_r^{\pm}(t,z)}{\partial t} = \frac{g_r \Gamma_r}{2}(1 - i\alpha_r)\left[n_r(t,z) - n_r^{\mathrm{tr}}\right]\mathcal{E}_r^{\pm}(t,z) \quad (2.1)$$

$$\frac{\partial n_r(t,z)}{\partial t} = \eta \frac{j_r(t,z)}{ed} - \gamma_r n_r(t,z) - v g_r \Gamma_r \left[n_r(t,z) - n_r^{\mathrm{tr}}\right] \sum_{\pm} |\mathcal{E}_r^{\pm}(t,z)|^2. \quad (2.2)$$

The dynamical variables are the left (+) and right (−) propagating slowly varying complex electric field amplitudes $\mathcal{E}_r^{\pm}$ and the carrier density n_r. In this model the slowly varying envelope approximation has been made, hence the total electric field is given by

$$E(t,z) \equiv \frac{1}{2}\left(\left(\mathcal{E}_r^{+}(t,z)\, e^{-ikz} + \mathcal{E}_r^{-}(t,z)\, e^{+ikz}\right) e^{-i\Omega_0 t} + c.c.\right), \quad (2.3)$$

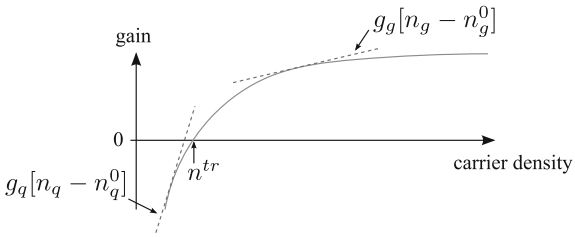

Fig. 2.1 Sketch of the carrier dependence of the gain for a semiconductor quantum-well material

where k is the reference wavenumber which is related to the optical frequency Ω_0 via the linear dispersion relation $k \equiv \Omega_0/v$, with group velocity v. To arrive at Eqs. (2.1) and (2.2) the polarisation has been adiabatically eliminated. This simplification is possible because semiconductor quantum-well lasers are generally of class B [29], meaning that the polarisation dephasing time is much faster than other time scales of the system.

The carrier–field interaction is described by the complex gain function

$$g_r \Gamma_r \left(1 - i\alpha_r\right) \left[n_r\left(t, z\right) - n_r^0\right], \tag{2.4}$$

which is the gain linearised about the carrier density at some operation point and written in terms of the effective transparency carrier density of this linearised function, n_r^0. The differential gain is given by g_r and transverse modal confinement is accounted for by the factor Γ_r. Carrier-induced refractive index changes are modelled by the amplitude-phase coupling factors α_r (linewidth enhancement factors). The factor of $1/2$ in Eq. (2.1) is included because expression (2.4) describes the intensity gain. In Fig. 2.1 a sketch of the carrier dependence of the gain is shown for a semiconductor quantum-well material [19, 30, 31]. If the same material is used for the gain ($r = g$) and absorber ($r = q$) sections then the difference in their gain comes from the difference in their carrier densities during operation. Due to the reverse bias the absorber section will always be below transparency. The operation range of the gain section will be at some higher carrier density due to the pump current. Therefore, for the gain and absorber section the gain function is linearised about different points, leading to different values for the differential gain g_r.

In Eq. (2.2) the injection of charge carriers is described by the pump current density j_r. Included in the pump term are the injection efficiency factor η, the electron charge e and the thickness of the active region d. The lifetime of charge carriers in the quantum-well states is limited by non-radiative scattering processes, which are included via the carrier decay rate γ_r. Inspection of the carrier–field interaction term in Eq. (2.2) shows that the electric field is scaled to the dimensions $(\text{length})^{-3/2}$ such that $|\mathcal{E}_r^{\pm}|^2$ gives the photon density.

A two section passively mode-locked laser consists of two active sections, a gain section which is electrically pumped and an absorber section which is negatively biased. Depending on the geometry of the laser, passive sections could also be included. For the derivation of the DDE model a ring cavity geometry must be assumed. A schematic of such a cavity is shown in Fig. 2.2. Equations (2.1) and (2.2) are applied in each section of the laser cavity. The index $r \in \{g, q, p\}$ is used to

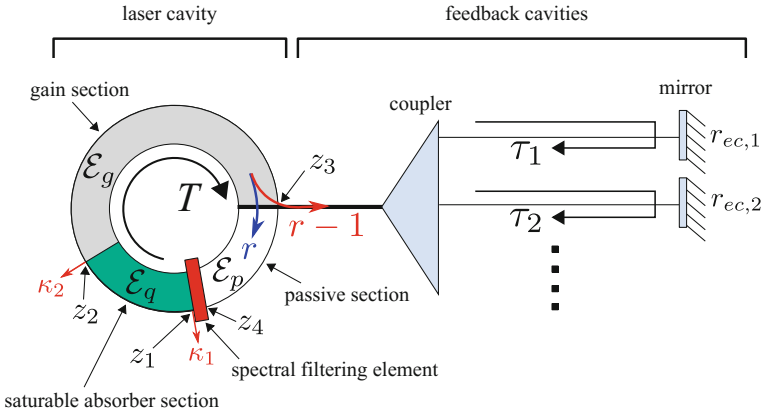

Fig. 2.2 Schematic diagram of a ring-cavity laser subject to optical feedback from multiple external cavities

denote the gain, absorber and passive sections, respectively. In the passive section there are no carriers, hence the evolution of the electric field envelope is described solely by Eq. (2.1) with the right-hand side equal to zero. In the absorber section $j_q = 0$ holds, and the influence of the applied reverse bias is manifested in the carrier decay rate γ_q and the gain of this section (Eq. (2.4)). A lumped-element approach is used to include non-resonant losses at the facets between each of the sections (κ_1 and κ_2 in Fig. 2.2). Mirror losses as well as coupling to and from the feedback cavities is included between the gain and passive sections. Also using a lumped-element approach, a filtering element $\hat{f}(\omega)$ is included between the passive and absorber sections (red bar in Fig. 2.2). The purpose of this filter is to account for the finite width of the gain spectrum. The z-direction is chosen along the axis of the cavity and is the propagation direction of longitudinal modes of the laser. Along with the ring cavity geometry, the second main assumption of the DDE model is unidirectional propagation of the light field. Here clockwise propagation is chosen, i.e. $\mathcal{E}_r^- = 0$ and $\mathcal{E}_r^+ = \mathcal{E}$. The validity and implications of these two assumptions will be discussed in Sect. 2.3.

Including the losses and feedback contributions as described above, the boundary conditions between each of the sections are

$$\mathcal{E}_g(t, z_2) = \sqrt{\kappa_2}\mathcal{E}_q(t, z_2), \tag{2.5}$$

$$\mathcal{E}_p(t,z_3) = \sqrt{r}\mathcal{E}_g(t,z_3) + (1-r)\sum_{n=1}^{N}\left(\sum_{l=1}^{\infty} r^{(l-1)/2}k_n^l r_{ec,n}^{l/2}\mathcal{E}_g(t-l\tau_n,z_3)\,e^{ilC_n}\right)$$
$$+ (1-r)\sum_{n=1}^{N}\sum_{n'\neq n}\left(\sum_{l=1}^{\infty} r^{l/2}k_n^l r_{ec,n}^{l/2}k_{n'}r_{ec,n'}^{1/2}\mathcal{E}_g(t-\tau_{n'}-l\tau_n,z_3)\,e^{i(C_{n'}+lC_n)}\right)$$
$$+ (1-r)\sum_{n=1}^{N}\sum_{n'\neq n}\left(\sum_{l=1}^{\infty} r^{(l+1)/2}k_n^l r_{ec,n}^{l/2}k_{n'}^2 r_{ec,n'}\mathcal{E}_g(t-2\tau_{n'}-l\tau_n,z_3)\,e^{i(2C_{n'}+lC_n)}\right)$$
$$+\cdots \tag{2.6}$$

and

$$\hat{\mathcal{E}}_q(\omega,z_1+L) = \sqrt{\kappa_1}\hat{f}(\omega)\,\hat{\mathcal{E}}_p(\omega,z_1+L) = \sqrt{\kappa_1}\hat{f}(\omega)\,\hat{\mathcal{E}}_p(\omega,z_4)\,. \tag{2.7}$$

In Eqs. (2.5) and (2.7) κ_1 and κ_2 account for the internal non-resonant loss. These depend on the length of the active sections according to $\kappa_x = e^{-aL_x}$, where a is a loss rate per unit length and L_x is the length of the active section for which the losses are being accounted for.

In Eq. (2.6) feedback contributions from an arbitrary number N of external feedback cavities has been included. To experimentally implement such a feedback scheme there are several options. These include using beam-splitters or optical couplers to distribute the light among the feedback cavities [16, 32, 33]. Here we do not choose a particular scheme, but rather account for this with the factor k_n which gives the percentage of the light coupled into feedback cavity $n \in \{1, 2, .., N\}$, with $\sum_{n=1}^{N} k_n = 1$. The sum over l accounts for feedback contributions after multiple roundtrips in the feedback cavities. Also included are contributions from light that has made roundtrips in different feedback cavities. The reflectivity of the end facets of each of the feedback cavities is given by $r_{ec,n}$. This factor primarily determines the feedback strength. The fast oscillating reference frequency Ω_0 also plays a role in the feedback terms, as due to these fast oscillations a phase shift can accumulate with respect to the light in the laser cavity. This can be understood by considering the delayed electric field $E(t-\tau,z_3) = \mathcal{E}_r^+(t-\tau,z_3)\,e^{-ikz_3}e^{-i\Omega_0(t-\tau)}$ at the out-coupling facet (position z_3). Over the delay time τ a phase shift of $\Omega_0\tau$ accumulates. For each of the feedback cavities the phase shift per roundtrip is then given by $C_n \equiv \Omega_0\tau_n$. Since the optical frequency $\Omega_0\tau$ is very large (THz) very small changes in the delay times τ_n results in variations in the phase that are greater than 2π. Due to this we can essentially treat the feedback phase independently from the delay time. In Eqs. (2.5)–(2.7) the non-resonant losses and reflectivities are all given with respect to the intensity, hence the respective electric field losses are given by the square root of these terms.

In the limit of weak feedback, i.e. small external cavity reflectivities $r_{ec,n}$, the feedback terms in Eq. (2.6) can be simplified by making the approximation that contributions after multiple roundtrips in the feedback cavities are negligible. Including only the terms that correspond to one roundtrip in a feedback cavity Eq. (2.6) becomes

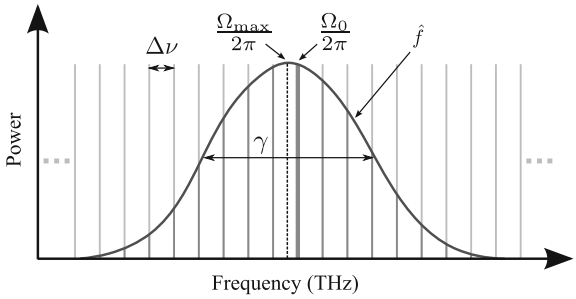

Fig. 2.3 Schematic diagram of the optical spectrum of a semiconductor mode-locked laser. The *light grey lines* indicate the cavity modes and the *dark grey lines* indicate the modes that can lase. The *black curve* represents the spectral filter that is applied to account for the frequency dependence of the gain

$$\mathcal{E}_p(t, z_3) = \sqrt{r}\mathcal{E}_g(t, z_3) + \sqrt{r}\sum_{n=1}^{N} K_n \mathcal{E}_g(t - \tau_n, z_3)\, e^{iC_n}, \tag{2.8}$$

where

$$K_n \equiv (1 - r)k_n \left(r_{ec,n}/r\right)^{1/2}. \tag{2.9}$$

In the boundary condition Eq. (2.7), $\hat{\mathcal{E}}_r$ is the Fourier transformed electric field and ω is the angular frequency. In this boundary condition several assumptions are made. Firstly, the filtering element is assumed to be infinitesimally thin, meaning that $z_1 = z_4$. Secondly, since $z_1 + L = z_4$ in the ring cavity geometry, the boundary conditions are periodic, i.e.

$$\mathcal{E}_r(t, z) = \mathcal{E}_r(t, z + L), \tag{2.10}$$

where L is the length of the laser cavity. The laser cavity modes are therefore restricted to

$$\Omega_L = n\frac{2\pi v}{L} \tag{2.11}$$

for $n = 1, 2, 3, \ldots$. All modes fulfilling this condition can exist in the laser cavity. This is shown schematically in Fig. 2.3. The grey lines in this diagram indicate modes with a spacing of $\Delta\nu = T'^{-1} = \frac{v}{L}$, where T' is the cold cavity roundtrip time. Without a spectral filter, according to Eqs. (2.1) and (2.2), all of these modes are equally amplified and would have the same output power. However in real devices only a finite number of modes will have positive net gain [34, 35]. The spectral filter (black curve) is added to account for this by increasing the losses for modes away from the maximum gain mode. In the derivation of the DDE model a Lorentzian shaped filter is chosen;

$$\hat{f}(\omega) \equiv \frac{\gamma}{\gamma + i(\omega - \Delta\Omega)}. \tag{2.12}$$

This expression is written in the frame of the slowly varying amplitude, i.e. the optical frequencies are given by $\omega' = \Omega_0 + \omega$. $\Delta\Omega \equiv \Omega_0 - \Omega_{\max}$ is the detuning between

the frequency of the maximum of the filter $\Omega_{\max}$ and the reference optical frequency. The full-width at half maximum of the filter is given by γ. This parameter determines the number of modes that participate in the mode-locking, which is roughly given by $\gamma T'$ [12]. The Lorentzian filter shape is chosen as it allows the derivation of a system of delay differential equations.

Before applying the boundary conditions it is useful to make a change of coordinates to a frame co-moving with the electric field: $(t, z) \mapsto \left(t', z'\right)$ with $t' = t - z/v$ and $z' = z/v$. In this coordinate system Eqs. (2.1)–(2.2), applied to each section of the laser, are given by

$$\frac{\partial A_r}{\partial z'} = \frac{1}{2}\left(1 - i\alpha_r\right) N_r\left(t', z'\right) A_r\left(t', z'\right), \tag{2.13}$$

$$\frac{\partial N_g}{\partial t'} = \mathcal{J}_g\left(t', z'\right) - \gamma_g N_g\left(t', z'\right) - N_g\left(t', z'\right) |A_g\left(t', z'\right)|^2 \tag{2.14}$$

and

$$\frac{\partial N_q}{\partial t'} = -\mathcal{J}_q\left(t', z'\right) - \gamma_q N_q\left(t', z'\right) - \tilde{r}_s N_q\left(t', z'\right) |A_q\left(t', z'\right)|^2, \tag{2.15}$$

with $N_p\left(t', z'\right) \equiv 0$. Here the dynamical variables have been rescaled such that $A_r \equiv \sqrt{v g_g \Gamma_g}\mathcal{E}_r$ and $N_r \equiv v g_r \Gamma_r [n_r - n_r^0]$. Accordingly, the rescaled pump parameters are $\mathcal{J}_g \equiv v g_g \Gamma_g \left(j_g - \gamma_g n_g^0\right)$ and $\mathcal{J}_q \equiv v g_q \Gamma_q \gamma_q n_q^0$, and the saturation energy ratio $\tilde{r}_s \equiv g_q \Gamma_q / g_g \Gamma_g$ has been introduced [36, 37]. The saturation energies describe how much energy must be absorbed or emitted for the absorber and gain sections to become transparency. The ratio of these energies is a crucial parameter; for mode-locking to occur the absorber must have a smaller saturation energy than the gain section, i.e. $\tilde{r}_s > 1$ as the saturation energies are proportional to $(g_r \Gamma_r)^{-1}$.

In this co-moving frame the evolution of the electric field amplitude along the sections of the laser is now described by ordinary differential equations (Eq. (2.13)). Integrating these equations over each section yields

$$A_q\left(t', z_2'\right) = e^{-\frac{1}{2}\left(1 - i\alpha_q\right) Q\left(t'\right)} A_q\left(t', z_1'\right), \tag{2.16}$$

$$A_g\left(t', z_3'\right) = e^{\frac{1}{2}\left(1 - i\alpha_g\right) G\left(t'\right)} A_g\left(t', z_2'\right) \tag{2.17}$$

and

$$A_p\left(t', z_3'\right) = A_p\left(t', z_4'\right), \tag{2.18}$$

where

$$Q\left(t'\right) \equiv -\int_{z_1'}^{z_2'} N_q\left(t', z'\right) dz' \quad \text{and} \quad G\left(t'\right) \equiv \int_{z_2'}^{z_3'} N_g\left(t', z'\right) dz'$$

are the dimensionless carrier densities integrated over the absorber and gain sections, which we shall refer to as the gain and losses, respectively. Next, the boundary conditions can be applied to obtain the evolution of the electric field amplitude over one roundtrip in the laser cavity. Using Eqs. (2.5) and (2.8), transformed to the co-moving frame, the evolution from $A_q\left(t', z_1'\right)$ to $A_p\left(t', z_4'\right)$ is given by

$$A_p\left(t', z_4'\right) = \sqrt{r\kappa_2} e^{\frac{1}{2}(1-i\alpha_g)G(t')-\frac{1}{2}(1-i\alpha_q)Q(t')} A_q\left(t', z_1'\right) + \sqrt{r\kappa_2}\sum_{n=1}^{N} K_n e^{iC_n} e^{\frac{1}{2}(1-i\alpha_g)G(t'-\tau_n)-\frac{1}{2}(1-i\alpha_q)Q(t'-\tau_n)} A_q\left(t'-\tau_n, z_1'\right). \tag{2.19}$$

In order to apply Eq. (2.7), it must first be transformed to the time domain and the co-moving frame. The transformation to the time domain is done using the convolution theorem which states

$$\mathcal{F}[g * h\,(t)] = \mathcal{F}[g\,(t)]\mathcal{F}[h\,(t)], \tag{2.20}$$

where g and h are functions of t, $\mathcal{F}$ is the Fourier transform and $(*)$ denotes a convolution product. In the co-moving frame, and in terms of the rescaled field, Eq. (2.7) can now be rewritten as

$$\begin{aligned} A_q\left(t'-T', z_1'+T'\right) &= \sqrt{\kappa_1}\left(f\left(t'-T'\right) * A_p\left(t'-T', z_4'\right)\right) \\ &= \sqrt{\kappa_1}\int_{-\infty}^{t'-T'} f\left(t'-T'-\theta\right) A_p\left(\theta, z_4'\right) d\theta, \end{aligned} \tag{2.21}$$

once again T' is the cold cavity roundtrip time given by L/v. The upper limit of the integral has been set to $t'-T'$, instead of infinity, in order to preserve causality. This is done under the assumption that $A_q\left(\theta, z_4'\right) = 0$ for $\theta > t'-T'$. Substituting Eq. (2.19) into Eq. (2.21) yields

$$A_q\left(t', z_1'\right) = \int_{-\infty}^{t'-T'} f\left(t'-T'-\theta\right) R\,(\theta)\, A_q\left(\theta, z_1'\right) d\theta + \sum_{n=1}^{N} K_n e^{iC_n} \int_{-\infty}^{t'-T'} f\left(t'-T'-\theta\right) R\,(\theta-\tau_n)\, A_q\left(\theta-\tau_n, z_1'\right) d\theta, \tag{2.22}$$

where we have defined

$$R\,(\theta) \equiv \sqrt{\kappa} e^{\frac{1}{2}(1-i\alpha_g)G(\theta)-\frac{1}{2}(1-i\alpha_q)Q(\theta)} \tag{2.23}$$

which describes the gain and losses accumulated over one roundtrip in the laser cavity. Here we also define $\kappa \equiv \kappa_1\kappa_2 r$. This parameter accounts for all the non-

resonant and mirror losses per roundtrip. To obtain the left hand side of Eq. (2.22) the periodic boundary condition has been applied, which in the co-moving coordinates is expressed as

$$A_q\left(t', z_1'\right) = A_q\left(t' - T', z_1' + T'\right). \tag{2.24}$$

The form of which can be derived by substituting $z + L$ for z in the transformation, i.e. $(t, z + L) \mapsto \left(t - \frac{(z+L)}{v}, \frac{(z+L)}{v}\right) = \left(t' - T', z' + T'\right)$.

The evolution of the field over one roundtrip is now expressed entirely in terms of the electric field amplitude in the saturable absorber section at position z_1', which we relabel $A\left(t'\right) \equiv A_q\left(t', z_1'\right)$. In order to obtain a differential equation for the time evolution of $A\left(t'\right)$ Eq. (2.22) is differentiated with respect to t'. To do this we first substitute in the filtering function, which in the time domain is written as

$$f\left(t'\right) \equiv \gamma e^{(-\gamma + i\Delta\Omega)t'}. \tag{2.25}$$

With some slight rearrangement this yields

$$\begin{aligned} A\left(t'\right) e^{(\gamma - i\Delta\Omega)t'} = &\int_{-\infty}^{t'-T'} \gamma e^{(\gamma - i\Delta\Omega)(T+\theta)} R\left(\theta\right) A\left(\theta\right) d\theta \\ &+ \sum_{n=1}^{N} K_n e^{iC_n} \int_{-\infty}^{t'-T'} \gamma e^{(\gamma - i\Delta\Omega)(T+\theta)} R\left(\theta - \tau_n\right) A\left(\theta - \tau_n\right) d\theta. \end{aligned} \tag{2.26}$$

Differentiating Eq. (2.26) then results in a DDE for the time evolution of $A\left(t'\right)$;

$$\begin{aligned} \frac{dA}{dt'} + \left(\gamma - i\Delta\Omega\right) A\left(t'\right) = &\gamma R\left(t' - T'\right) A\left(t' - T'\right) \\ &+ \gamma \sum_{n=1}^{N} K_n e^{iC_n} R\left(t' - T' - \tau_n\right) A\left(t' - T' - \tau_n\right). \end{aligned} \tag{2.27}$$

To obtain differential equations for the time evolution of the integrated carrier densities $G\left(t'\right)$ and $Q\left(t'\right)$, we integrate Eqs. (2.14) and (2.15) over the gain and absorber sections, respectively:

$$\frac{\partial G}{\partial t'} = J_g\left(t'\right) - \gamma_g G\left(t'\right) - \int_{z_2}^{z_3} N_g\left(t', z'\right) |A_g\left(t', z'\right)|^2 dz', \tag{2.28}$$

$$\frac{\partial Q}{\partial t'} = J_q\left(t'\right) - \gamma_q Q\left(t'\right) + \tilde{r}_s \int_{z_1}^{z_2} N_q\left(t', z'\right) |A_q\left(t', z'\right)|^2 dz'. \tag{2.29}$$

Here we have introduced the unsaturated gain and absorption parameters

$$J_g\left(t'\right) \equiv \int_{z_2}^{z_3} \mathcal{J}_g\left(t', z'\right) dz' \tag{2.30}$$

and

$$J_q\left(t'\right) \equiv \int_{z_1}^{z_2} \mathcal{J}_q\left(t', z'\right) dz', \tag{2.31}$$

respectively. To express the integrals in Eqs. (2.28) and (2.29) in terms of $G\left(t'\right)$, $Q\left(t'\right)$ and $A\left(t'\right)$ we must make use of the equations describing the evolution of the field along the gain and absorber sections (Eqs. (2.13), (2.16) and (2.17), and boundary condition Eq. (2.5)). From Eq. (2.13) we obtain

$$A_r^* \frac{\partial A_r}{\partial z'} + A_r \frac{\partial A_r^*}{\partial z'} = \frac{1}{2}\left(1 - i\alpha_r\right) N_r A_r^* A_r + \frac{1}{2}\left(1 + i\alpha_r\right) N_r A_r A_r^* \tag{2.32}$$

by multiplying by the complex conjugate of the field amplitude A_r^* and adding the complex conjugate of Eq. (2.13) multiplied by A_r. This expression gives

$$\frac{\partial |A_r|^2}{\partial z'} = N_r\left(t', z'\right) |A_r\left(t', z'\right)|^2. \tag{2.33}$$

Integrating over the gain and absorber sections then gives

$$|A_{g,q}\left(t', z'_{3,2}\right)|^2 - |A_{g,q}\left(t', z'_{2,1}\right)|^2 = \int_{z'_{2,1}}^{z'_{3,2}} N_{g,q}\left(t', z'\right) |A_{g,q}\left(t', z'\right)|^2 dz'. \tag{2.34}$$

Using Eqs. (2.16), (2.17) and (2.5) the left hand side can be expressed in terms of $G\left(t'\right)$, $Q\left(t'\right)$ and $A\left(t'\right)$, which we then substitute into Eqs. (2.28) and (2.29) to obtain

$$\frac{\partial G}{\partial t'} = J_g\left(t'\right) - \gamma_g G\left(t'\right) - \kappa_2 e^{-Q\left(t'\right)}\left(e^{G\left(t'\right)} - 1\right)|A\left(t'\right)|^2 \tag{2.35}$$

and

$$\frac{\partial Q}{\partial t'} = J_q\left(t'\right) - \gamma_q Q\left(t'\right) - \tilde{r}_s e^{-Q\left(t'\right)}\left(e^{Q\left(t'\right)} - 1\right)|A\left(t'\right)|^2. \tag{2.36}$$

Equations (2.27), (2.35) and (2.36) now describe the evolution of the electric field amplitude at position z_1 and the gain and absorption per roundtrip in the laser cavity. As of yet the influence of spontaneous emission is not included. We treat this effect in a phenomenological manner by adding a complex Gaussian white noise term to the electric field equation (Eq. (2.27)). Adding this noise term and making the transformation $A\left(t'\right) \equiv \frac{1}{\sqrt{\kappa_2}} \mathcal{A}\left(t'\right) e^{i\Delta\Omega t'}$ we obtain the final system of coupled DDEs;

$$\frac{d\mathcal{A}}{dt'} = -\gamma\mathcal{A}\left(t'\right) + \gamma R\left(t' - T'\right)e^{-i\Delta\Omega T'}\mathcal{A}\left(t' - T'\right) + \sqrt{R_{sp}}\xi\left(t'\right) + \gamma\sum_{n=1}^{N} K_n e^{iC_n} R\left(t' - T' - \tau_n\right)e^{-i\Delta\Omega\left(T'+\tau_n\right)}\mathcal{A}\left(t' - T' - \tau_n\right), \quad (2.37)$$

$$\frac{\partial G}{\partial t'} = J_g\left(t'\right) - \gamma_g G\left(t'\right) - e^{-Q\left(t'\right)}\left(e^{G\left(t'\right)} - 1\right)|\mathcal{A}\left(t'\right)|^2 \quad (2.38)$$

and

$$\frac{\partial Q}{\partial t'} = J_q\left(t'\right) - \gamma_q Q\left(t'\right) - r_s e^{-Q\left(t'\right)}\left(e^{Q\left(t'\right)} - 1\right)|\mathcal{A}\left(t'\right)|^2. \quad (2.39)$$

Here the ratio of excitation energies has been rescaled, $r_s \equiv \tilde{r}_s/\kappa_2$. The noise strength is given by R_{sp} and $\xi\left(t'\right) = \xi_R + i\xi_I$ has the properties

$$\langle\xi_i\left(t'\right)\rangle = 0 \quad (2.40)$$

and

$$\langle\xi_i\left(t'\right)\xi_j\left(t''\right)\rangle = \delta_{i,j}\delta\left(t' - t''\right), \quad (2.41)$$

for $i, j \in \{R, I\}$.

2.2.1 Dimensionless Formulation of the DDE System

For numerical simulations it is convenient to rescale the DDE system such that the parameters are all dimensionless. In [12] the authors do this by rescaling by the absorber recovery rate γ_q. We shall take the same approach as in [13] and use the cold cavity roundtrip time T'. This is a convenient time scale of the system to use when studying the system with feedback as features in the feedback delay time dependence vary on this time scale, as will be shown in the next chapter.

We write the dimensionless form of Eqs. (2.37)–(2.39) as

$$\frac{d\mathcal{E}}{dt} = -\gamma\mathcal{E}\left(t\right) + \gamma R\left(t - T\right)e^{-i\Delta\Omega T}\mathcal{E}\left(t - T\right) + \sqrt{R_{sp}}\xi\left(t\right) + \gamma\sum_{n=1}^{N} K_n e^{iC_n} R\left(t - T - \tau_n\right)e^{-i\Delta\Omega\left(T+\tau_n\right)}\mathcal{E}\left(t - T - \tau_n\right), \quad (2.42)$$

$$\frac{\partial G}{\partial t} = J_g\left(t\right) - \gamma_g G\left(t\right) - e^{-Q\left(t\right)}\left(e^{G\left(t\right)} - 1\right)|\mathcal{E}\left(t\right)|^2 \quad (2.43)$$

and

$$\frac{\partial Q}{\partial t} = J_q\left(t\right) - \gamma_q Q\left(t\right) - r_s e^{-Q\left(t\right)}\left(e^{Q\left(t\right)} - 1\right)|\mathcal{E}\left(t\right)|^2, \quad (2.44)$$

where time has been rescaled as $t = t'/T'$, the cold cavity roundtrip time is now $T = T'/T' = 1$ and $\mathcal{E} = \sqrt{T'}\mathcal{A}$. For the other parameters we use the same symbols as in Eqs. (2.37)–(2.39), but they now represent the rescaled quantities. All times are rescaled by dividing by T' and all rates are rescaled by multiplying by T'. $R(t)$ is as defined in Eq. (2.23).

For all the numerical simulations we use the dimensionless form of the DDE system and all for results that will be presented in the subsequent chapters, we will refer to the dimensionless parameter values.

2.2.2 Parameter Values

In this subsection we will briefly discuss some of the final parameters of the DDE model (Eqs. (2.42)–(2.44)) and the values that will be used.

In an experiment the tunable parameters that determine the light output of a passively mode-locked laser are the pump current that is injected into the gain section and the reverse bias which is applied to the absorber section. In our final system of equations these control parameters are related to J_g in Eq. (2.43) and J_q and γ_q in Eq. (2.44). J_g is related to the pump current, but not directly as it referenced to the current needed to achieve transparency in the gain section, i.e. it is proportional to the excess pump current. In the absorber section the applied bias modifies the energy barrier which needs to be overcome for carriers to escape the quantum-well [38]. This influences the carrier recovery rate γ_q and hence the carrier density about which the gain should be linearised. The carrier recovery rate γ_q, the differential gain g_q and the effective transparency carrier density n_q^0 all enter into the unsaturated absorption parameter J_q, meaning that the bias dependence is manifested in J_q and γ_q.

In the subsequent chapters will we see that the amplitude-phase coupling factors, α_g and α_q, can strongly influence the dynamics. These parameters are included to account for carrier-induced refractive index changes and are proportional to $\frac{\partial(\delta n)/\partial N}{\partial g/\partial N}$, where δn is the carrier-induced refractive index change and $\partial g/\partial N$ is the differential gain [19]. For quantum-well based gain media δn and g depend non-linearly on the carrier densities leading to carrier dependent α-factors. In the model presented here these factors are assumed to be constant. We will partially account for the carrier dependence of the α-factors by investigating scenarios where the values are different in the gain and absorber sections. However, our default values for α_g and α_q will be zero.

For the charge-carrier recovery rates we will use values that are typical for semiconductor quantum-well materials. In the gain section the carrier lifetimes can typically range from 0.1 to 1 ns [39–41]. In the absorber section the carrier lifetimes are lower due to the reverse bias which sweeps out the carriers. Typical values which can be found in the literature are in the range 5–50 ps [42]. However, in both cases the recovery times strongly depend on the structure of the gain material.

Table 2.1 Parameter values used in numerical simulations, unless stated otherwise

Parameter	Value	Dimensionless	Parameter	Value	Dimensionless
T	25 ps	1	γ	2.66 ps^{-1}	66.5
γ_g	1 ns^{-1}	0.025	γ_q	75 ns^{-1}	1.875
J_g	0.12 ps^{-1}	3.0	J_q	0.3 ps^{-1}	7.5
r_s	25.0	25.0	C_m	0	0
κ	0.1	0.1	$\Delta\Omega$	0	0
α_g	0	0	α_q	0	0

The parameter values that we will use throughout this thesis, unless stated otherwise, are those given in Table 2.1. We choose a cold-cavity roundtrip time of 25 ps, which results in a repetition rate of about 40 GHz in the fundamental mode-locking regime. For a linear cavity, this roundtrip time corresponds to a length of about 1 mm, which is a typical length for a passively mode-locked semiconductor laser [16, 43, 44].

2.3 Discussion of the DDE Model

The main assumptions made to be able to derive the DDE system (Eqs. (2.37)–(2.39)) are that the laser has a ring cavity geometry and that the propagation of light is unidirectional. This approach has been widely, and successfully, employed to study the dynamics of various laser systems. These include hybrid mode-locked lasers [45, 46], passively mode-locked lasers with optical injection [47–49] or optical feedback [13, 18, 50, 51] and Fourier domain mode-locking [52]. In many of these cases experimental comparison is made with devices that have a linear cavity geometry and bidirectional propagation. Despite this difference the DDE models have been shown to reproduce the qualitative behaviour of the dynamics very well [16, 33, 45, 48]. There are however still some qualitative differences that will be discussed in this section.

In [53] the authors numerically study a travelling-wave model for a monolithic-semiconductor passively mode-locked laser with a linear cavity geometry. The carrier and field equations are the same as those used in the DDE model and spectral filtering is also included in a lumped element approach, i.e. the essential difference between the DDE system of [12] and the travelling-wave system of [53] is the laser-cavity geometry and hence that in the latter case there are two counter-propagating fields. The bifurcation diagrams for these two systems are qualitatively very similar. The main difference that arises is in the 2nd harmonic mode-locking regime. In this regime there are two pulses travelling in the laser cavity. In the linear-cavity model these two pulses collide, which leads to faster saturation of the medium at the point of the collision. For the cavity model used in [53], this collision takes place in the

gain section. This is unfavourable for mode-locking and consequently leads to a break-up of the symmetry of the pulses (period doubling bifurcation). The heights and separation of the pulses change such that the collision only occurs in the gain section every second roundtrip, thereby reducing the saturation of the gain section. This is not observed in the DDE model as the two pulses cannot interact.

In a linear cavity pulse interaction can also occur in the fundamental mode-locking regime. As the pulse is reflected at the end facets there is an interaction between the forward and backward moving parts of the pulse, this again leads to faster saturation of the medium at the point of interaction. This effect is utilised in the so-called self-colliding-pulse mode-locking, where the saturable absorber is placed near the high reflectivity facet to increase its modulation [41]. Such interaction effects in the fundamental mode-locking regime are also not present in the DDE model. There are however other factors related to the geometry of the cavity, which have been shown to have a greater influence on the modulation of the absorber section, that can be observed in the DDE model. In [5] the effect of the positioning of the saturable absorber in a two section laser, i.e. whether or not the absorber is located at the end of the cavity with the anti-reflection coated facet, is studied using a travelling-wave model. Here the authors predict that the output power of the pulses is increased, the pulse widths are decreased and the amplitude and timing jitter is reduced, when the absorber is placed in front of the anti-reflection coated facet. The reasoning for this is that despite a reduction in the interaction of the counter-propagating fields due to the reduced reflectivity, the power of the pulse impinging on the absorber from the gain section is now much greater since there are less mirror losses at the end of the gain section. This leads to faster saturation of the absorber [54], which is known to improve the mode-locking properties [1]. This dependence on the absorber position has subsequently been demonstrated experimentally [55, 56]. In the DDE model similar effects can be observed by placing the out-coupling losses before or after the absorber section [7].

Depending on the heterostructure of the laser under investigation, refinements can be made to the DDE model by choosing more sophisticated models for the carriers. In [7, 50, 57] the respective authors have used the DDE approach with charge-carrier equations tailored to quantum-dot lasers. However, comparisons between the results that will be presented in the subsequent sections, and those present in [50], show that the qualitative trends of the feedback dependence are the same for the simple DDE we use (Eqs. (2.42)–(2.44)) and the more complicated quantum-dot based DDE models.

Aside from the ring-cavity geometry and the unidirectional propagation, there are other simplifying assumptions that mean that the DDE model can only be used to make qualitative not quantitative predicts for experiments. One of these is the lumped-element approach to including the internal non-resonant losses. By including the internal losses only at the ends of the gain and absorber sections the electric field is larger than it should be as it propagates through these sections, which affects the dynamics of the charge carriers. This can be improved upon by dividing the gain and absorber in to multiple sections and including internal losses between each section. The authors of [7] have done this for a quantum-dot mode-locked laser and have

shown that by adding more sections to the ring cavity they obtained better agreement with a travelling-wave model for an equivalent linear cavity. This is however at the expense of a greater computational cost, as each added section requires an additional carrier equation.

References

1. H.A. Haus, Theory of mode locking with a slow saturable absorber. IEEE J. Quantum Electron. **11**, 736 (1975)
2. J. Mulet, J. Mørk, Analysis of timing jitter in external-cavity modelocked semiconductor lasers. IEEE J. Quantum Electron. **42**, 249 (2006)
3. E.A. Avrutin, B.M. Russell, Dynamics and spectra of monolithic mode-locked laser diodes under external optical feedback. IEEE J. Quantum Electron. **45**, 1456 (2009)
4. J. Javaloyes, S. Balle, Mode-locking in semiconductor Fabry-Pérot lasers. IEEE J. Quantum Electron. **46**(7), 1023–1030 (2010)
5. J. Javaloyes, S. Balle, Anticolliding design for monolithic passively modelocked semiconductor lasers. Opt. Lett. **36**, 4407–4409 (2011)
6. M. Rossetti, P. Bardella, I. Montrosset, Time-domain travelling-wave model for quantum dot passively mode-locked lasers. IEEE J. Quantum Electron. **47**, 139 (2011)
7. M. Rossetti, P. Bardella, I. Montrosset, Modeling passive mode-locking in quantum dot lasers: a comparison between a finite-difference traveling-wave model and a delayed differential equation approach. IEEE J. Quantum Electron. **47**, 569 (2011)
8. M. Radziunas, A. Vladimirov, E.A. Viktorov, G. Fiol, H. Schmeckebier, D. Bimberg, Pulse broadening in quantum-dot mode-locked semiconductor lasers: simulation, analysis, and experiments. IEEE J. Quantum Electron. **47**, 935–943 (2011)
9. H. Simos, C. Simos, C. Mesaritakis, D. Syvridis, Two-section quantum-dot mode-locked lasers under optical feedback: pulse broadening and harmonic operation. IEEE J. Quantum Electron. **48**, 872 (2012)
10. V. Moskalenko, J. Javaloyes, S. Balle, M.K. Smit, E.A.J.M. Bente, Theoretical study of colliding pulse passively mode-locked semiconductor ring lasers with an intracavity Mach–Zehnder modulator. IEEE J. Quantum Electron. **50**(6), 415–422 (2014)
11. A. Vladimirov, D.V. Turaev, G. Kozyreff, Delay differential equations for mode-locked semiconductor lasers. Opt. Lett. **29**, 1221 (2004)
12. A. Vladimirov, D.V. Turaev, Model for passive mode locking in semiconductor lasers. Phys. Rev. A **72**, 033808 (2005)
13. C. Otto, K. Lüdge, A. Vladimirov, M. Wolfrum, E. Schöll, Delay induced dynamics and jitter reduction of passively mode-locked semiconductor laser subject to optical feedback. New J. Phys. **14**, 113033 (2012)
14. S. Sanders, A. Yariv, J. Paslaski, J.E. Ungar, H.A. Zarem, Passive mode locking of a two-section multiple quantum well laser at harmonics of the cavity round-trip frequency. Appl. Phys. Lett. **58**, 681–683 (1990)
15. U. Bandelow, M. Radziunas, A. Vladimirov, B. Hüttl, R. Kaiser, 40GHz mode locked semiconductor lasers: theory, simulation and experiments. Opt. Quantum Electron. **38**, 495 (2006)
16. D. Arsenijevic, M. Kleinert, D. Bimberg, Phase noise and jitter reduction by optical feedback on passively mode-locked quantum-dot lasers. Appl. Phys. Lett. **103**, 231101 (2013)
17. M. Marconi, J. Javaloyes, S. Balle, M. Giudici, How lasing localized structures evolve out of passive mode locking. Phys. Rev. Lett. **112**(22), 223901 (2014)
18. C. Otto, L.C. Jaurigue, E. Schöll, K. Lüdge, Optimization of timing jitter reduction by optical feedback for a passively mode-locked laser. IEEE Photonics J. **6**, 1501814 (2014)
19. W.W. Chow, S.W. Koch, *Semiconductor-Laser Fundamentals* (Springer, Berlin, 1999)

20. B. Lingnau, W.W. Chow, E. Schöll, K. Lüdge, Feedback and injection locking instabilities in quantum-dot lasers: a microscopically based bifurcation analysis. New J. Phys. **15**, 093031 (2013)
21. B. Lingnau, W.W. Chow, K. Lüdge, Amplitude-phase coupling and chirp in quantum-dot lasers: influence of charge carrier scattering dynamics. Opt. Express **22**, 4867–4879 (2014)
22. B. Lingnau, K. Lüdge, Analytic characterization of the dynamic regimes of quantum-dot lasers. Photonics **2**, 402–413 (2015)
23. A. Vladimirov, D.V. Turaev, New model for mode-locking in semiconductor lasers. Radiophys. Quantum Electron. **47**, 769–776 (2004)
24. A. Vladimirov, D. Rachinskii, M. Wolfrum, Modeling of passively modelocked semiconductor lasers, in *Nonlinear Laser Dynamics-From Quantum Dots to Cryptography, Reviews in Nonlinear Dynamics and Complexity*, ed. by K. Lüdge (Wiley, Weinheim, 2011), pp. 183–213
25. H. Haken, *Laser Theory* (Springer, New York, 1983)
26. B. Tromborg, H.E. Lassen, H. Olesen, Traveling wave analysis of semiconductor lasers: modulation responses, mode stability and quantum mechanical treatment of noise spectra. IEEE J. Quantum Electron. **30**, 939 (1994)
27. G.H.M. van Tartwijk, G.P. Agrawal, Laser instabilities: a modern perspective. Prog. Quantum Electron. **22**, 43–122 (1998)
28. E. Schöll, Dynamic theory of picosecond optical pulse shaping by gain-switched semiconductor laser amplifiers. IEEE J. Quantum Electron. **24**, 435–442 (1988)
29. F.T. Arecchi, G.L. Lippi, G.P. Puccioni, J.R. Tredicce, Deterministic chaos in laser with injected signal. Opt. Commun. **51**, 308–315 (1984)
30. M. Asada, A. Kameyama, Gain and intervalence band absorption in quantum-well lasers. IEEE J. Quantum Electron. **20**, 745–753 (1984)
31. K.Y. Lau, P.L. Derry, A. Yariv, Ultimate limit in low threshold quantum well GaAlAs semiconductor lasers. Appl. Phys. Lett. **52**, 88–90 (1987)
32. M. Haji, L. Hou, A.E. Kelly, J. Akbar, J.H. Marsh, J.M. Arnold, C.N. Ironside, High frequency optoelectronic oscillators based on the optical feedback of semiconductor mode-locked laser diodes. Opt. Express **20**, 3268–3274 (2012)
33. O. Nikiforov, L.C. Jaurigue, L. Drzewietzki, K. Lüdge, S. Breuer, Experimental demonstration of change of dynamical properties of a passively mode-locked semiconductor laser subject to dual optical feedback by dual full delay-range tuning. Opt. Express **24**, 14301–14310 (2016)
34. J.P. Hohimer, G.A. Vawter, Passive mode locking of monolithic semiconductor ring lasers at 86 GHz. Appl. Phys. Lett. **63**, 1598–1600 (1993)
35. A.A. Ukhanov, A. Stintz, P.G. Eliseev, K.J. Malloy, Comparison of the carrier induced refractive index, gain, and linewidth enhancement factor in quantum dot and quantum well lasers. Appl. Phys. Lett. **84**, 1058–1060 (2004)
36. H. Haus, Mode-locking of lasers. IEEE J. Sel. Top. Quantum Electron. **6**, 1173–1185 (2000)
37. C. Otto, *Dynamics of Quantum Dot Lasers-Effects of Optical Feedback and External Optical Injection, Springer Theses* (Springer, Heidelberg, 2014)
38. D.B. Malins, A. Gomez-Iglesias, S.J. White, W. Sibbett, A. Miller, E.U. Rafailov, Ultrafast electroabsorption dynamics in an InAs quantum dot saturable absorber at 1.3μm. Appl. Phys. Lett. **89**, 171111 (2006)
39. E.O. Göbel, H. Jung, J. Kuhl, K. Ploog, Recombination enhancement due to carrier localization in quantum well structures. Phys. Rev. Lett. **51**, 1588–1591 (1983)
40. J. Hader, J.V. Moloney, S.W. Koch, Structural dependence of carrier capture time in semiconductor quantum-well lasers. Appl. Phys. Lett. **85**, 369–371 (2004)
41. D.J. Jones, L.M. Zhang, J.E. Carroll, D. Marcenac, Dynamics of monolithic passively mode-locked semiconductor lasers. IEEE J. Quantum Electron. **31**, 1051–1058 (1995)
42. J.R. Karin, R.J. Helkey, D.J. Derickson, R. Nagarajan, D.S. Allin, J.E. Bowers, R.L. Thornton, Ultrafast dynamics in field-enhanced saturable absorbers. Appl. Phys. Lett. **64**, 676–678 (1994)
43. G. Fiol, M. Kleinert, D. Arsenijevic, D. Bimberg, 1.3μm range 40 GHz quantum-dot mode-locked laser under external continuous wave light injection or optical feedback. Semicond. Sci. Technol. **26**, 014006 (2011)

44. G. Fiol, 1.3μm Monolithic Mode-Locked Quantum-Dot Semiconductor Laser, PhD thesis. (Technische Universität Berlin, 2011)
45. G. Fiol, D. Arsenijevic, D. Bimberg, A. Vladimirov, M. Wolfrum, E.A. Viktorov, P. Mandel, Hybrid mode-locking in a 40 GHz monolithic quantum dot laser. Appl. Phys. Lett. **96**, 011104 (2010)
46. R.M. Arkhipov, A.S. Pimenov, M. Radziunas, D. Rachinskii, A. Vladimirov, D. Arsenijevic, H. Schmeckebier, D. Bimberg, Hybrid mode locking in semiconductor lasers: simulations, analysis, and experiments. IEEE J. Quantum Electron. **19**(4), 1100208 (2013)
47. N. Rebrova, G. Huyet, D. Rachinskii, A. Vladimirov, Optically injected mode-locked laser. Phys. Rev. E **83**, 066202 (2011)
48. A.S. Pimenov, E.A. Viktorov, S.P. Hegarty, T. Habruseva, G. Huyet, D. Rachinskii, A. Vladimirov, Bistability and hysteresis in an optically injected two-section semiconductor laser. Phys. Rev. A **89**, 052903 (2014)
49. T. Habruseva, D. Arsenijevic, M. Kleinert, D. Bimberg, G. Huyet, S.P. Hegarty, Optimum phase noise reduction and repetition rate tuning in quantum-dot mode-locked lasers. Appl. Phys. Lett. **104**, 1–4 (2014)
50. C. Simos, H. Simos, C. Mesaritakis, A. Kapsalis, D. Syvridis, Pulse and noise properties of a two section passively mode-locked quantum dot laser under long delay feedback. Opt. Commun. **313**, 248–255 (2014)
51. L.C. Jaurigue, O. Nikiforov, E. Schöll, S. Breuer, K. Lüdge, Dynamics of a passively mode-locked semiconductor laser subject to dual-cavity optical feedback. Phys. Rev. E **93**, 022205 (2016)
52. S. Slepneva, B. Kelleher, B. O'Shaughnessy, S.P. Hegarty, A. Vladimirov, G. Huyet, Dynamics of Fourier domain mode-locked lasers. Opt. Express **21**, 19240–19251 (2013)
53. A. Vladimirov, A.S. Pimenov, D. Rachinskii, Numerical study of dynamical regimes in a monolithic passively mode-locked semiconductor laser. IEEE J. Quantum Electron. **45**, 462–468 (2009)
54. H. Simos, C. Mesaritakis, T. Xu, P. Bardella, I. Montrosset, D. Syvridis, Numerical analysis of passively mode-locked quantum-dot lasers with absorber section at the low-reflectivity output facet. IEEE J. Quantum Electron. **49**, 3–10 (2013)
55. V. Moskalenko, K.A. Williams, E.A.J.M. Bente, Integrated extended-cavity 1.5-μm semiconductor laser switchable between self- and anti-colliding pulse passive mode-locking configuration. IEEE J. Sel. Top. Quantum Electron. **21**, 1101306 (2015)
56. J.P. Zhuang, V. Pusino, Y. Ding, S.C. Chan, M. Sorel, Experimental investigation of anti-colliding pulse mode-locked semiconductor lasers. Opt. Lett. **40**, 617–620 (2015)
57. A. Vladimirov, U. Bandelow, G. Fiol, D. Arsenijevic, M. Kleinert, D. Bimberg, A.S. Pimenov, D. Rachinskii, Dynamical regimes in a monolithic passively mode-locked quantum dot laser. J. Opt. Soc. Am. B **27**, 2102 (2010)

http://www.springer.com/978-3-319-58873-5

Passively Mode-Locked Semiconductor Lasers
Dynamics and Stochastic Properties in the Presence of
Optical Feedback

Jaurigue, L.

2017, XV, 196 p. 133 illus., 53 illus. in color., Hardcover
ISBN: 978-3-319-58873-5